Supporting Information

A Closed-loop and Scalable Process for Production of Biomass-derived Superhydrophilic Carbon for Supercapacitors

Rong Fu[a], Chang Yu*[a], Shaofeng Li[a], Jinhe Yu[a], Zhao Wang[a], Wei Guo[a], Yuanyang Xie[a], Le Yang[a], Kunlun Liu[a], Weicheng Ren[a] and Jieshan Qiu* [a,b]

[a]*State Key Lab of Fine Chemicals, School of Chemical Engineering, Liaoning Key Lab for Energy Materials and Chemical Engineering, Dalian University of Technology, Dalian 116024, China*

[b]*College of Chemical Engineering, Beijing University of Chemical Technology, Beijing, China*

**Corresponding author: E-mail: chang.yu@dlut.edu.cn (C. Yu) ; carbon@dlut.edu.cn (J. S. Qiu)*

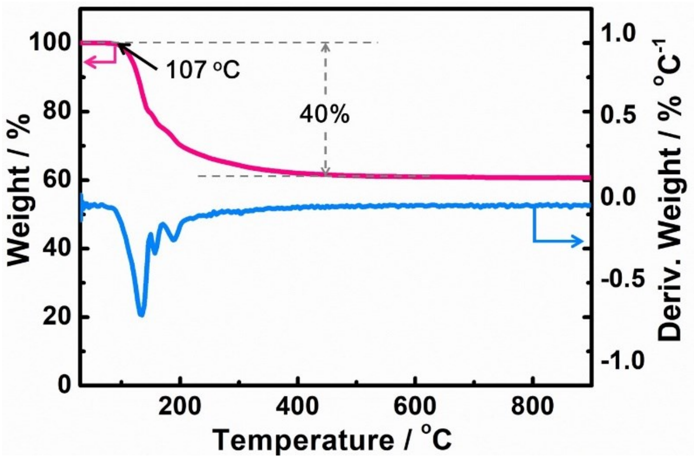

Fig. S1. Thermogravimetric analysis (TGA) and differential thermogravimetry (DTG) curves of boric acid in a N_2 atmosphere.

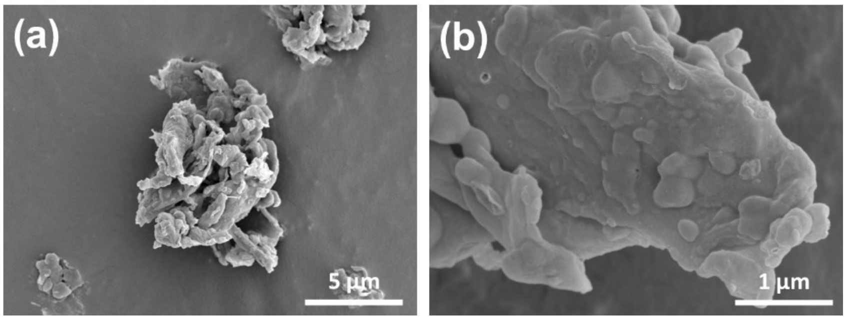

Fig. S2. (a, b) SEM images of DFC.

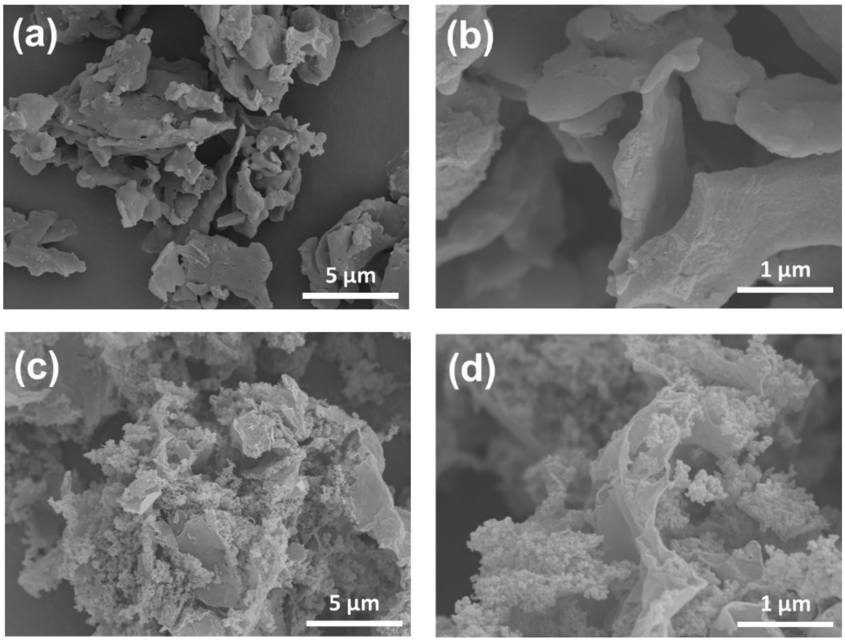

Fig. S3. SEM images of (a, b) $B_{0.5}$-SC and (c, d) B_3-SC.

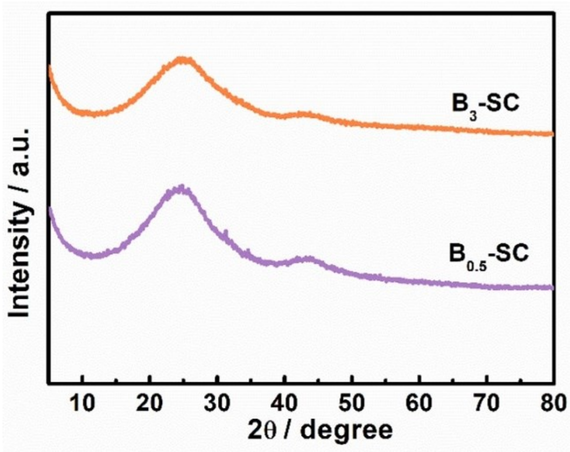

Fig. S4. XRD patterns of $B_{0.5}$-SC and B_3-SC.

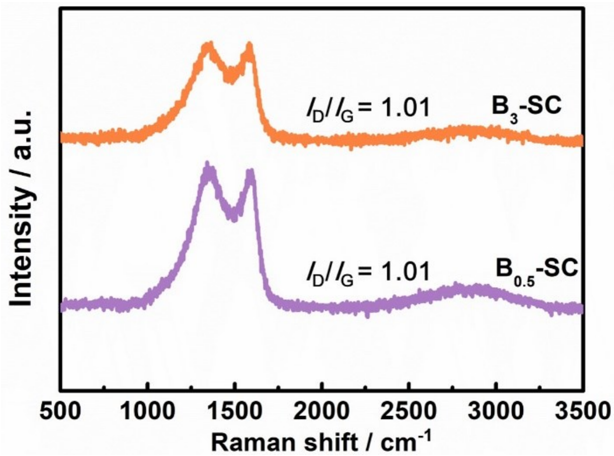

Fig. S5. Raman spectra of $B_{0.5}$-SC and B_3-SC.

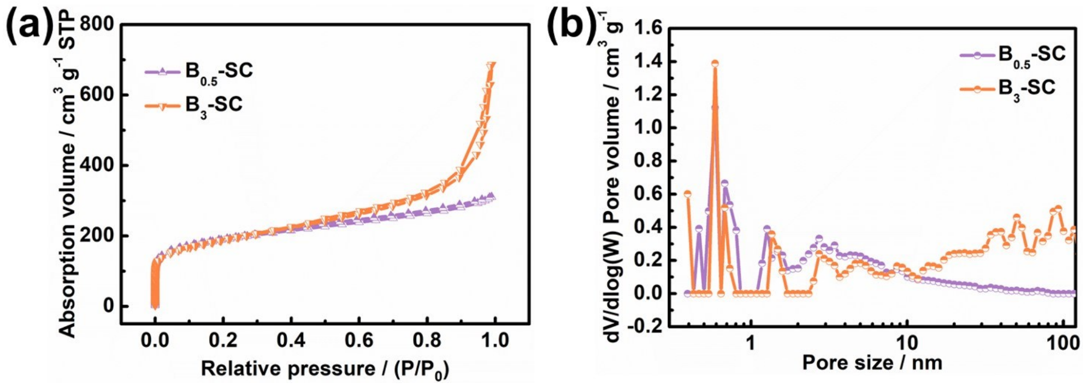

Fig. S6. (a) Nitrogen adsorption-desorption isotherms and (b) pore size distributions of $B_{0.5}$-SC and B_3-SC.

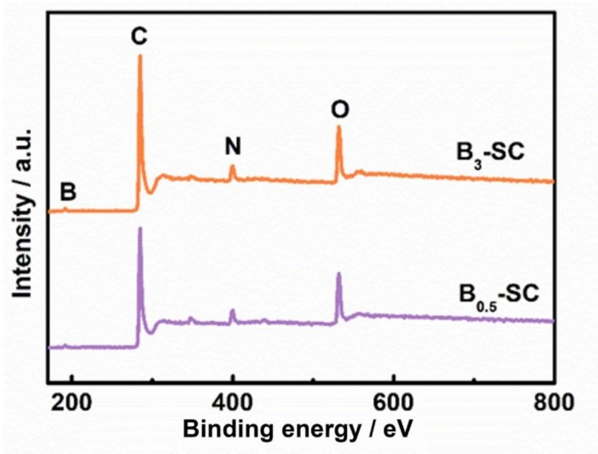

Fig. S7. XPS survey spectra of $B_{0.5}$-SC and B_3-SC.

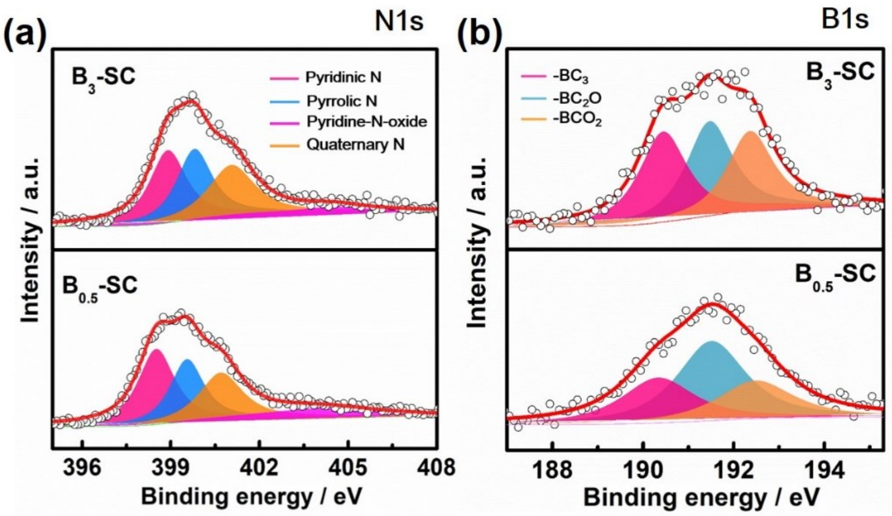

Fig. S8. High-resolution XPS spectra of (a) N 1s and (b) B 1s for $B_{0.5}$-SC and B_3-SC.

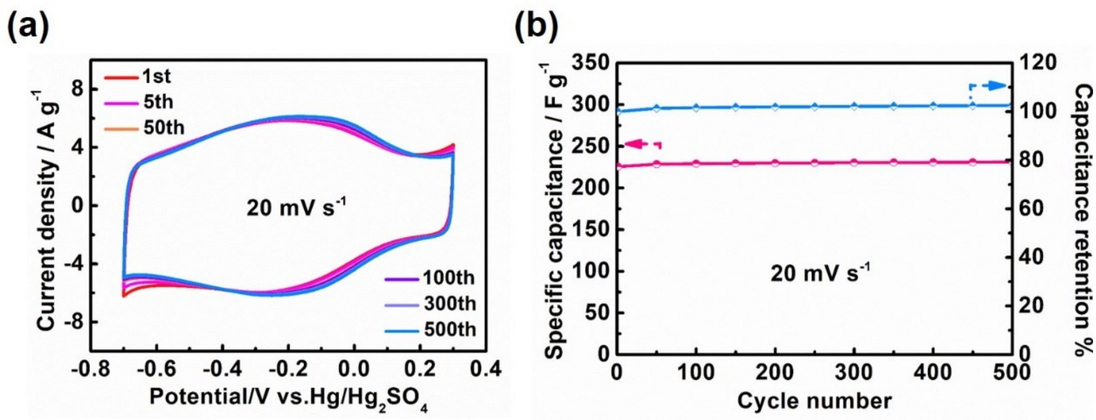

Fig. S9. (a) The CV curves of different cycle numbers and (b) cycling performance for B_1-SC at 20 mV s^{-1}.

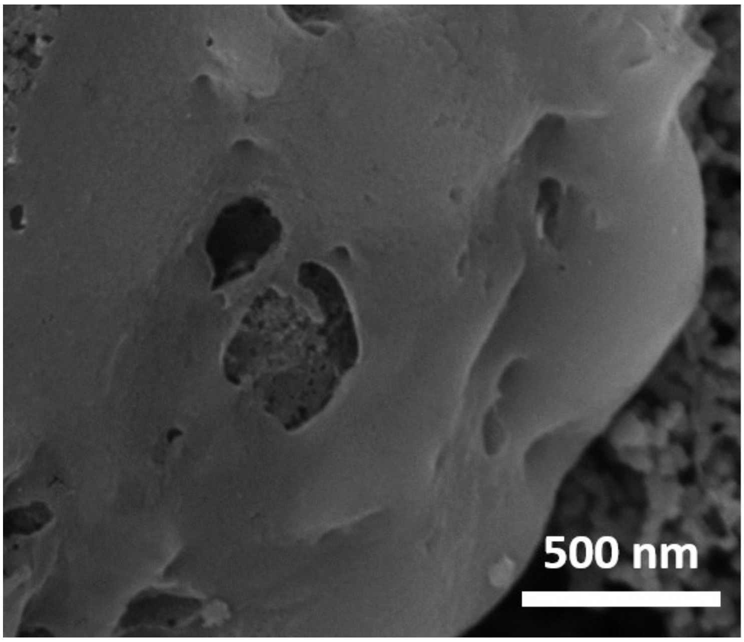

Fig. S10. SEM image of B_1-SC after CV cycling test.

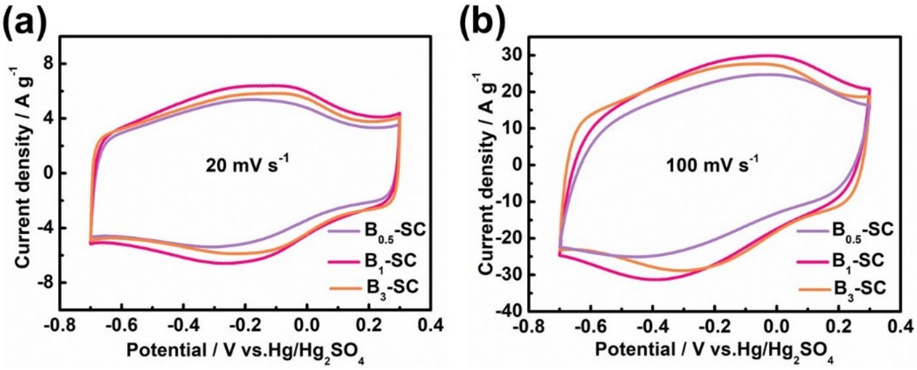

Fig. S11. The CV curves for $B_{0.5}$-SC, B_1-SC and B_3-SC at scan rates of (a) 20 mV s^{-1} and (b) 100 mV s^{-1}.

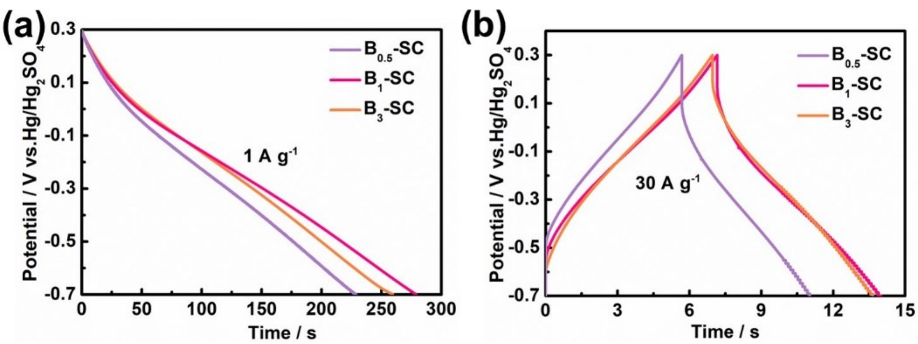

Fig. S12. The GC curves for $B_{0.5}$-SC, B_1-SC and B_3-SC at current densities of (a) 1 A g^{-1} and (b) 30 A g^{-1}.

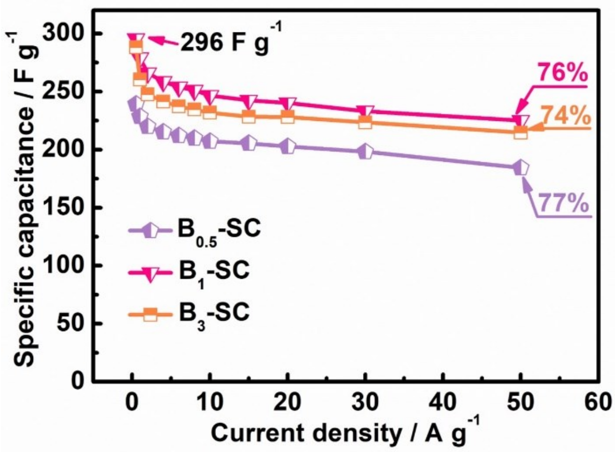

Fig. S13. The gravimetric specific capacitances for the $B_{0.5}$-SC, B_1-SC and B_3-SC at current densities from 0.5 to 50 A g^{-1}.

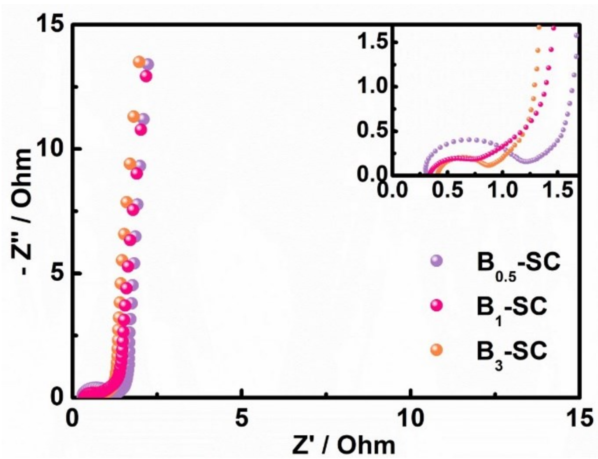

Fig. S14. Nyquist plots of the $B_{0.5}$-SC, B_1-SC and B_3-SC (inset: a magnification for the high-frequency region).

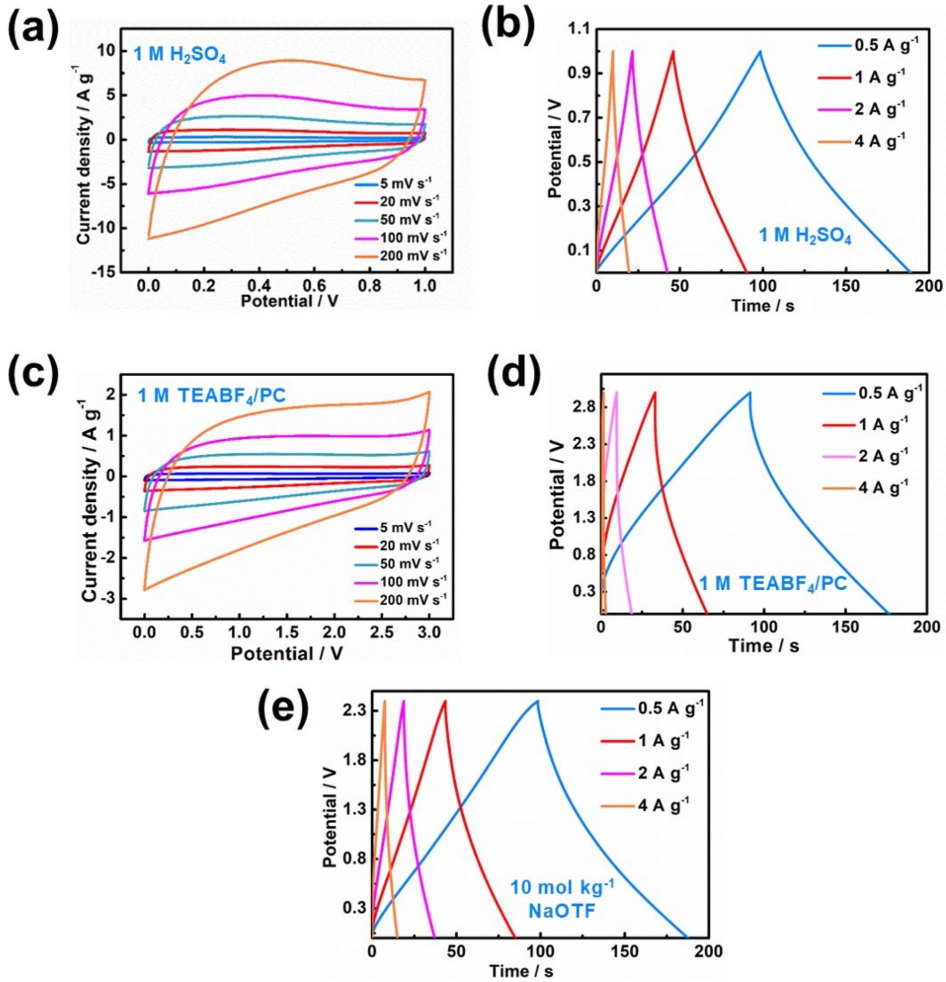

Fig. S15. Electrochemical performance of B_1-SC based symmetric supercapacitors in various electrolytes: CV curves at different scan rates from 5 to 200 mV s^{-1} with 1 M H_2SO_4 (a) and 1 M $TEABF_4$/PC (c), respectively; GC curves at various current densities of 0.5-4 A g^{-1} with 1 M H_2SO_4 (b), 1 M $TEABF_4$/PC (d) and 10 mol kg^{-1} NaOTF (e), respectively.

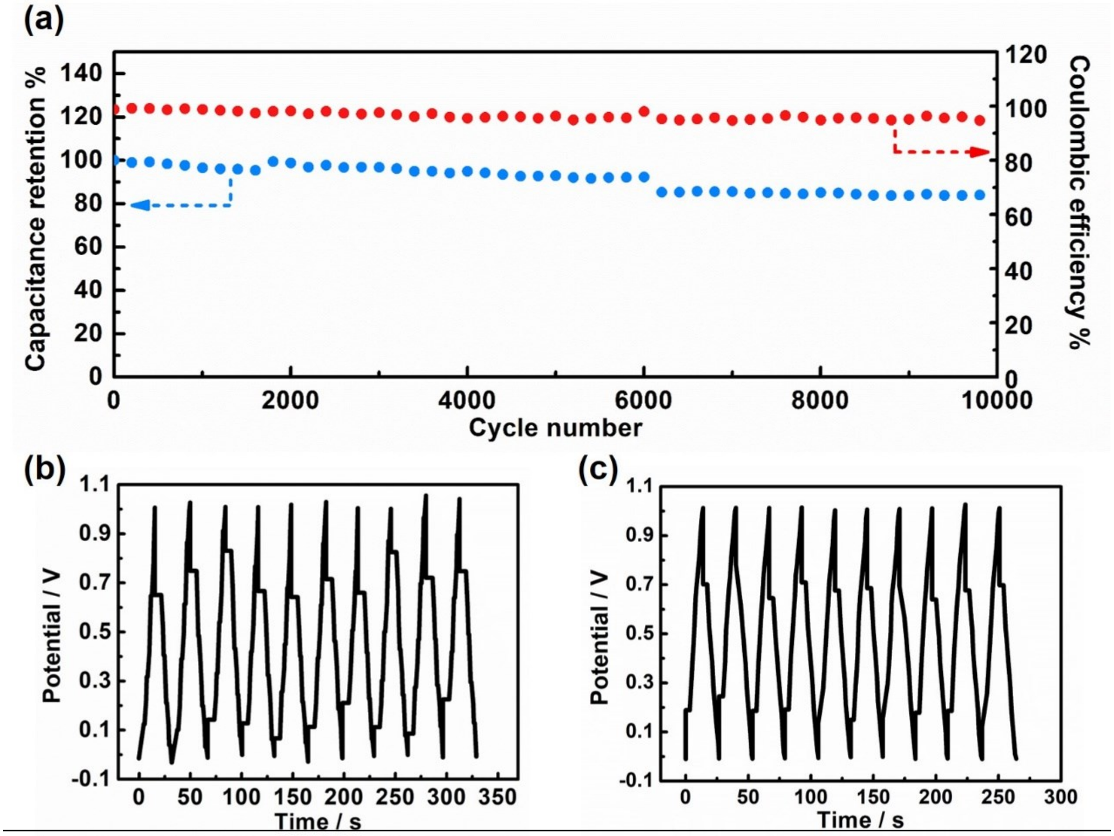

Fig. S16. (a) The cycling performance of B_1-SC for the symmetric supercapacitor with 1 M H_2SO_4 at 4 A g^{-1}. The first ten cycles (b) and last ten cycles (c) of GC curves.

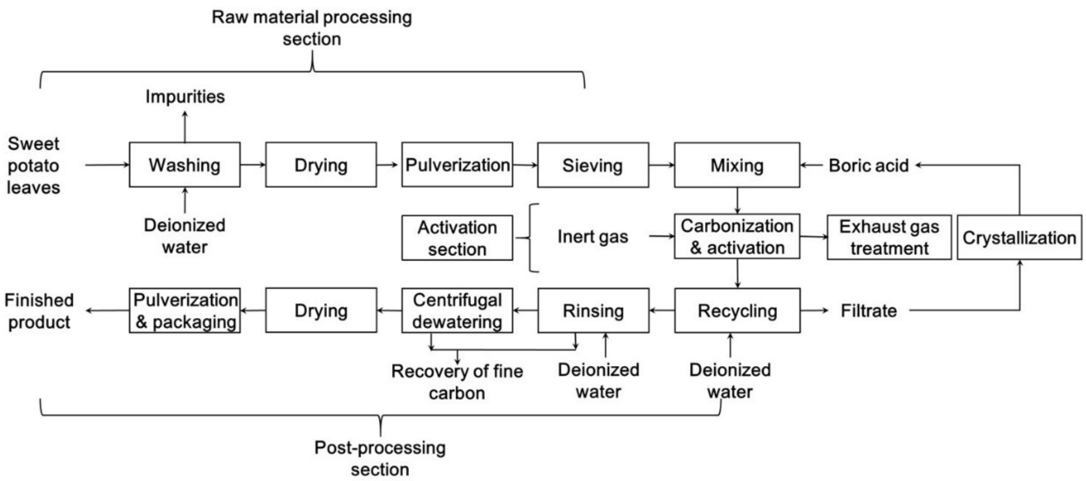

Fig. S17. The process flow chart of scalable and green production for B_1-SC.

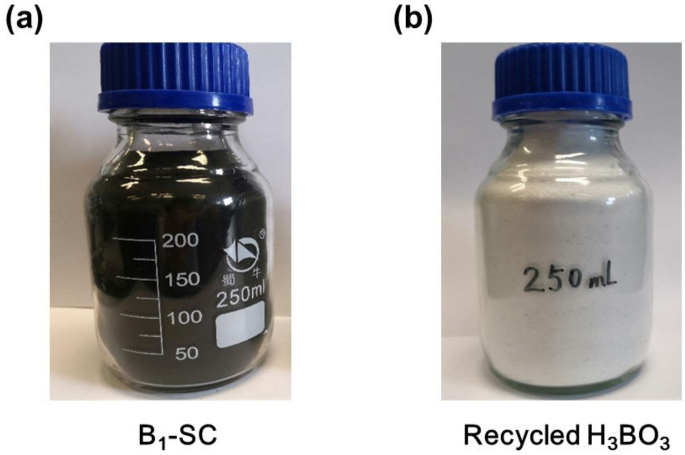

Fig. S18. The digital photograph of (a) the B_1-SC black product and (b) recycled boric acid.

Table S1. Pore structure parameters of DFC, $B_{0.5}$-SC, B_1-SC and B_3-SC measured by N_2 adsorption–desorption isotherms.

Sample	S_{BET} [a] ($m^2 g^{-1}$)	V_{total} [b] ($cm^3 g^{-1}$)	V_{micro} [c] ($cm^3 g^{-1}$)	V_{meso} [d] ($cm^3 g^{-1}$)	W_d [e] (nm)	V_{micro}/V_{total} [f] %	V_{meso}/V_{total} [g] %	V_{macro}/V_{total} [h] %
DFC	1073	0.63	0.28	0.17	7.7	44	27	29
$B_{0.5}$-SC	676	0.37	0.18	0.15	4.8	49	41	10
B_1-SC	844	0.55	0.20	0.20	6.9	36	36	28
B_3-SC	668	0.54	0.12	0.10	11.1	22	19	59

[a] Specific surface area calculated by BET method. [b] Total pore volume calculated by DFT method. [c] Micropore volume (DFT, pore size < 2 nm). [d] Mesopore volume (DFT, 2 nm < pore size < 50 nm). [e] Adsorption average pore diameter. [f] Percentage of micropore volume in total pore volume (DFT). [g] Percentage of mesopore volume in total pore volume (DFT). [h] Percentage of macropore volume in total pore volume (DFT).

Table S2. Percentages of carbon, oxygen, boron and nitrogen elements in DFC, $B_{0.5}$-SC, B_1-SC and B_3-SC derived from XPS analysis (based on the atomic ratio).

Sample	C at%	O at%	B at%	N at%
DFC	86.78	8.77	/	4.45
$B_{0.5}$-SC	74.40	14.15	4.94	6.51
B_1-SC	73.46	13.88	5.94	6.72
B_3-SC	77.05	12.63	4.25	6.07

Table S3. Total N content and the percentages of different N species in DFC, $B_{0.5}$-SC, B_1-SC and B_3-SC derived from the XPS analysis.

Sample	N_{total} [a] at%	N-6 [b] %	N-5 [c] %	N-Q [d] %	N-X [e] %
DFC	4.34	1.30	1.43	1.17	0.43
$B_{0.5}$-SC	6.48	2.33	1.81	1.68	0.65
B_1-SC	6.69	1.34	2.61	2.21	0.54
B_3-SC	6.05	2.06	1.94	1.82	0.24

[a] Total N content. [b] Pyridinic N (N-6). [c] Pyrrolic N (N-5). [d] Quanternary N (N-Q). [e] Pyridine-N-oxide (N-X).

Table S4. A comparasion of reported symmetric carbon based aqueous supercapacitors with our B_1-SC capacitor.

Sample	Electrolyte	Capacitances or Energy density	Current densities or Power density	Measurement configuration	Ref.
B_1-SC	1 M H_2SO_4	181 F g^{-1} 6.0 Wh kg^{-1}	0.5 A g^{-1} 1.0 kW kg^{-1}	2-Electrode	This work
B/N–carbon nanosphere	1 M H_2SO_4	60 F g^{-1} 2.1 Wh kg^{-1}	0.5 A g^{-1} 2.7 kW kg^{-1}	2-Electrode	1
N-doped porous biochar	1 M H_2SO_4	147 F g^{-1} 76 F g^{-1}	0.05 A g^{-1} 10 A g^{-1}	2-Electrode	2
HPCSLS	7 M KOH	104 F g^{-1} 3.6 Wh kg^{-1}	20 A g^{-1} 5.7 kW kg^{-1}	2-Electrode	3
G/CNTs-200	1 M Na_2SO_4	33 F g^{-1} 8.2 Wh kg^{-1}	2 mV s^{-1} 0.9 kW kg^{-1}	2-Electrode	4
BCN	1 M H_2SO_4	228 F g^{-1} 7.9 Wh kg^{-1}	1 A g^{-1} 0.2 kW kg^{-1}	2-Electrode	5
BMG-h	1 M H_2SO_4	122 F g^{-1}	1 A g^{-1}	2-Electrode	6
B-rGO	1 M H_2SO_4	240 F g^{-1}	0.5 A g^{-1}	3-Electrode	7
NPOC	0.5 M H_2SO_4	215 F g^{-1} 123 F g^{-1}	1 mV s^{-1} 80 A g^{-1}	3-Electrode	8
LGPCN	6 M KOH	11.7 Wh kg^{-1}	0.03 kW kg^{-1}	2-Electrode	9

Equation S1. The possible redox reactions for the N-configurations (1)-(3), O-functional groups (4) and (5) as well as B species (6) in the acidic electrolyte, which refers to the literature[1-9].

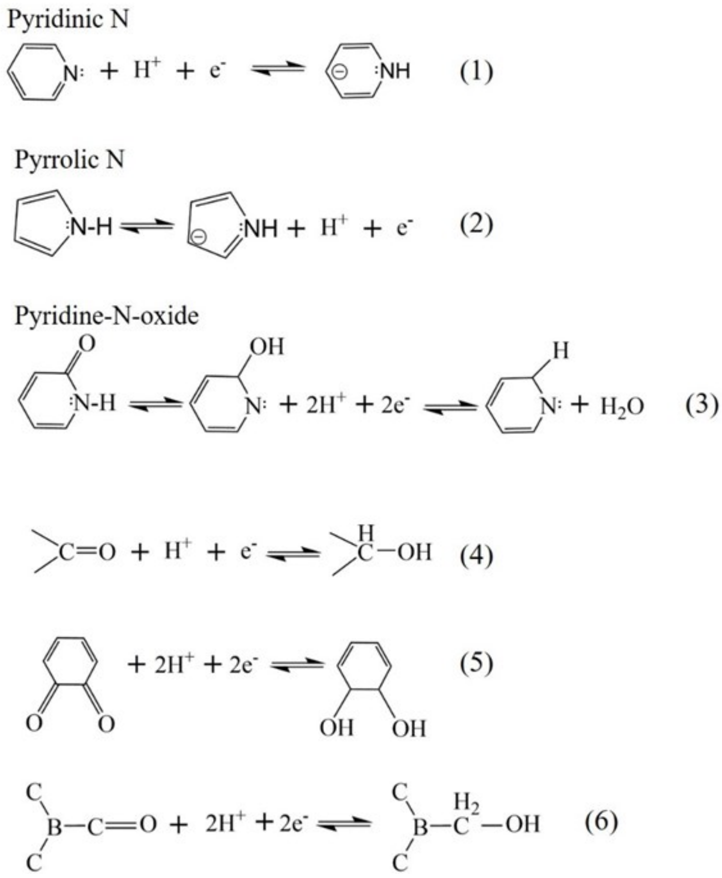

1. J. Hao, J. Wang, S. Qin, D. Liu, Y. Li and W. Lei, *J. Mater. Chem. A*, 2018, **6**, 8053-8058.
2. M. Zhang, C. Yu, Z. Ling, J. Yu, S. Li, C. Zhao, H. Huang and J. Qiu, *Green Chem.*, 2019, **21**, 2095-2103.
3. J. Pang, W. Zhang, J. Zhang, G. Cao, M. Han and Y. Yang, *Green Chem.*, 2017, **19**, 3916-3926.
4. B. Ding, D. Guo, Y. Wang, X. Wu and Z. Fan, *J. Power Sources*, 2018, **398**, 113-119.
5. A. K. Thakur, M. Majumder, R. B. Choudhary and S. B. Singh, *J. Power Sources*, 2018, **402**, 163-173.
6. R. Nankya, J. Lee, D. O. Opar and H. Jung, *Appl. Surf. Sci.*, 2019, **489**, 552-559.
7. T. Zhu, S. Li, B. Ren, L. Zhang, L. Dong and L. Tan, *J. Mater. Sci.*, 2019, **54**, 9632-9642.
8. C. Cui, Y. Gao, J. Li, C. Yang, M. Liu, H. Jin, Z. Xia, L. Dai, Y. Lei, J. Wang and S. Wang, *Angew. Chem. Int. Ed.*, 2020, **59**, 7928-7933.
9. Q. Niu, K. Gao, Q. Tang, L. Wang, L. Han, H. Fang, Y. Zhang, S. Wang and L. Wang, *Carbon*, 2017, **123**, 290-298.